

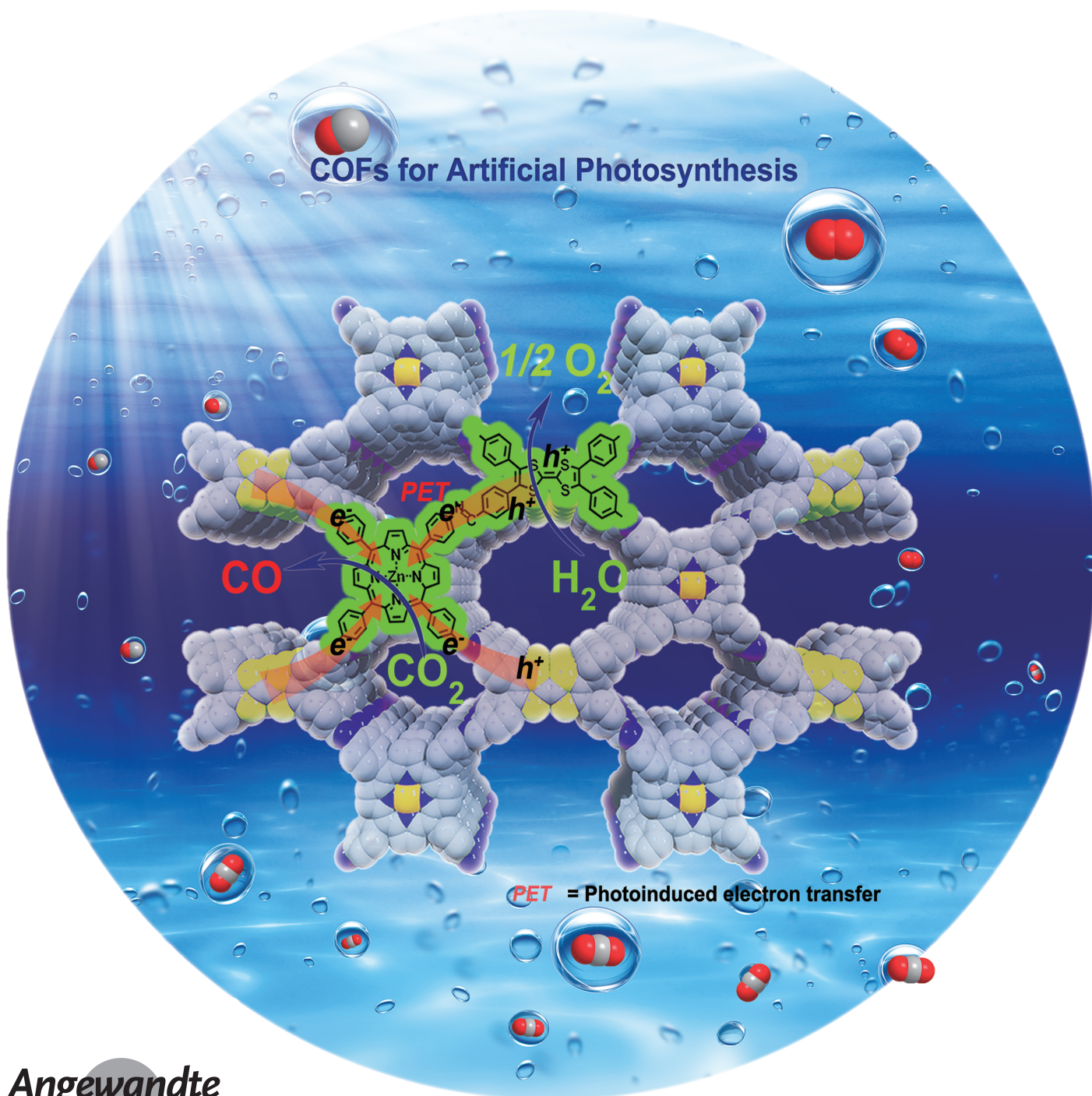


Photosynthesis Hot Paper

International Edition: DOI: 10.1002/anie.201906890
German Edition: DOI: 10.1002/ange.201906890

Rational Design of Crystalline Covalent Organic Frameworks for Efficient CO₂ Photoreduction with H₂O

Meng Lu⁺, Jiang Liu⁺, Qiang Li, Mi Zhang, Ming Liu, Jin-Lan Wang, Da-Qiang Yuan, and Ya-Qian Lan*



Abstract: Solar energy-driven conversion of CO_2 into fuels with H_2O as a sacrificial agent is a challenging research field in photosynthesis. Herein, a series of crystalline porphyrin-tetrathiafulvalene covalent organic frameworks (COFs) are synthesized and used as photocatalysts for reducing CO_2 with H_2O , in the absence of additional photosensitizer, sacrificial agents, and noble metal co-catalysts. The effective photo-generated electrons transfer from tetrathiafulvalene to porphyrin by covalent bonding, resulting in the separated electrons and holes, respectively, for CO_2 reduction and H_2O oxidation. By adjusting the band structures of TTCOFs, TTCOF-Zn achieved the highest photocatalytic CO production of $12.33 \mu\text{mol}$ with circa 100% selectivity, along with H_2O oxidation to O_2 . Furthermore, DFT calculations combined with a crystal structure model confirmed the structure–function relationship. Our work provides a new sight for designing more efficient artificial crystalline photocatalysts.

The excessive emission of carbon dioxide (CO_2) into the atmosphere from the burning of fossil fuels has caused severe energy and environmental issues that need to be solved urgently.^[1] It is well-known that the significance of plant photosynthesis lies in its ability to convert CO_2 and H_2O into carbohydrates and O_2 by using sunlight. Consequently, artificial photosynthesis is expected to mimic the above-mentioned process efficiently for reducing CO_2 with H_2O as electron donor, that is, integrating the CO_2 reduction reaction (CO_2RR) and H_2O oxidation half-reactions in one catalytic system, in which the development of photocatalysts is the most crucial factor.^[2] However, it is a daunting work to enable these two half-reactions to couple and interact effectively. At present, only very limited strategies on the design of efficient photocatalysts can realize the overall reaction, such as Z-scheme heterojunctions, which still face many problems.^[3] Therefore, it is essential to explore new photocatalytic systems with unambiguous structure for conducting the full photosynthetic reaction so as to obtain more insights into the structure–function relationship and then promote the development of this field.

Crystalline porous materials can provide a favorable structure–function research platform (including catalytic active site, charge transfer, and reaction mechanism) for

artificial photosynthesis because their well-defined structures can be elaborately designed and constructed by selecting appropriate building blocks or structural components according to specific demands.^[4] Nevertheless, the majority of crystalline porous materials are assembled with coordination bonds such as metal–organic frameworks (MOFs) and few of them strong enough for performing the overall reaction (i.e., reducing CO_2 with H_2O as electron donor).^[5] In contrast, covalent organic frameworks (COFs) with directional structural designability and high structural and chemical stabilities are a class of more promising porous crystalline materials for artificial photosynthesis.^[6] Additionally, COFs, with robust structures, are able to afford permanent platforms for catalytic active sites^[7] as well as large surface areas to fix CO_2 ,^[8] and their ordered π -array structures can provide pre-organized pathways for high-rate charge-carrier transport through delicate design.^[9] Taking these considerations into account, it is feasible to build a multifunctional COF photocatalyst systems in which the integration of CO_2 reduction and H_2O oxidation half-reactions can be implemented. Unfortunately, to the best of our knowledge, few such system has been investigated in crystalline COF materials field up to now.^[10]

Herein, a series of crystalline 2D rigid porphyrin-tetrathiafulvalene COFs (TTCOF-M, M = 2H, Zn, Ni, Cu) were designed for artificial photosynthesis including CO_2 reduction and H_2O oxidation. Electron-deficient metalloporphyrin (TAPP) complexes are known to have good visible-light collecting ability and potential CO_2 reduction performance,^[11] while electron-rich tetrathiafulvalene (TTF) has proven to be a superior electron donor with rapid electron transfer.^[12] Therefore, the effective covalent coupling between TAPP and TTF within COFs enables the visible-light driven electrons to efficiently separate and transfer from the TTF to TAPP moiety, resulting in that the photoexcited electrons (on porphyrin) and holes (on TTF) can be used for reduction and oxidation reactions, respectively. As expected, TTCOF-Zn/Cu COFs, owing to suitable photocatalytic redox potentials, were successfully used for reducing CO_2 with H_2O as electron donor, and TTCOF-Zn exhibited the highest CO production of $12.33 \mu\text{mol}$ and selectivity (ca. 100%) combined with excellent durability under our experimental conditions. Moreover, the corresponding DFT calculations agreed with the experimental results, which also gave detailed explanations about the charge-carrier transfer process and photocatalytic reaction pathways.

TTCOF-M was synthesized by Schiff-base condensation between metallized 5,10,15,20-tetrakis (4-aminophenyl)-porphyrinato] (TAPP-M, M = 2H, Zn, Ni, Cu) and 2,3,6,7-tetra (4-formylphenyl)-tetrathiafulvalene by solvothermal method (Figure 1a). The crystalline structure of TTCOF-M was determined by the powder X-ray diffraction (PXRD) combined with theoretical structural simulations using Materials Studio version 7.0. An orthorhombic $P222$ space group based on TTCOF-Zn was built and carried out Le Bail refinements of the PXRD patterns for full profile fitting against the proposed models, which provided a unit cell parameter of $a = 31.5694 \text{ \AA}$, $b = 21.9744 \text{ \AA}$, and $c = 5.0014 \text{ \AA}$, $\alpha = \beta = \gamma = 90^\circ$. The simulated PXRD pattern using AA stacking mode reproduced the experimentally observed curve while AB

[*] M. Lu,^[+] Dr. J. Liu,^[+] M. Zhang, M. Liu, Prof. Y.-Q. Lan
Jiangsu Collaborative Innovation Centre of Biomedical Functional Materials, School of Chemistry and Materials Science, Nanjing Normal University
No. 1, Wenyuan Road, Nanjing, 210023 (China)
E-mail: yqlan@njnu.edu.cn
Dr. Q. Li, Prof. J.-L. Wang
School of Physics, Southeast University
Nanjing 211189 (China)
Prof. D.-Q. Yuan
State Key Laboratory of Structural Chemistry Fujian Institute of Research on the Structure of Matter, Chinese Academy of Sciences Fuzhou, 350002 (China)

[+] These authors contributed equally to this work.

Supporting information and the ORCID identification number(s) for the author(s) of this article can be found under:
<https://doi.org/10.1002/anie.201906890>.

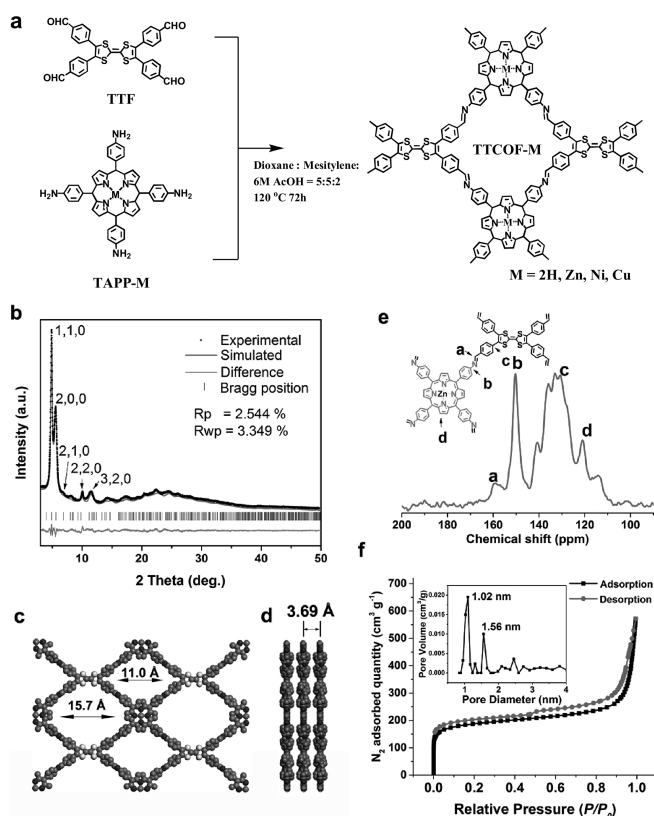


Figure 1. a) Schematic of the synthesis of TTCOF-M through the condensation of TTF and TAPP-M. b) Experimental (black dot) and simulated (red line) PXRD patterns of TTCOF-Zn c) Top and d) side views and e) ^{13}C ssNMR spectrum of TTCOF-Zn. f) N_2 adsorption curve of TTCOF-Zn at 77 K (inset pore-size distribution profile).

stacking did not, as revealed by a difference plot, with unweighted-profile R factor (R_p) = 2.544% and weighted-profile R factor (R_{wp}) = 3.349%, suggesting the validity of the computational model (Figure 1b). TTCOF-Zn has intense PXRD peaks at 4.98, 5.60, 6.9, 9.8, and 11.66°, which can be assigned to the 110, 200, 210, 220, and 320 faces, respectively. More details and raw data are given in the Supporting Information.

These refinements revealed that there is a dual channel along the c axis with theoretical pore sizes of 1.10 nm and 1.57 nm and a pore volume of $0.94\text{ cm}^3\text{ g}^{-1}$ (Figure 1c), and the distance between adjacent stacking 2D sheets is 3.69 Å (Figure 1d). Furthermore, the PXRD patterns of TTCOF-2H/Ni/Cu also showed high crystallinity (Figure S1–S3).

FTIR spectroscopy and ^{13}C solid-state NMR spectroscopy (^{13}C ssNMR) were used to confirm the chemical structure of TTCOF-M. In the FTIR spectra, the C=N stretching vibration band at 1620 cm^{-1} appeared in the resultant TTCOF-M, while the C=O stretching vibration band at 1700 cm^{-1} and $-\text{NH}_2$ vibration band at $3200\text{--}3500\text{ cm}^{-1}$ belonged to reactant monomers that decreased obviously^[13] (Figures S4 and S5). Furthermore, the characteristic peak of ca. 158.9 ppm in ^{13}C ssNMR corresponded to the carbon atom of the C=N bond^[14] (Figure 1e and Figures S6 and S7). These results confirmed the successful condensation reaction required for the TTCOF-M structure. X-ray photoelectron spectroscopy

(XPS) analysis results showed the divalent state of the central metal ion in porphyrin pocket of TTCOF-M ($M = \text{Zn}, \text{Ni}, \text{Cu}$) (Figure S8–S11).

The surface area and porosity of TTCOF-M were determined by N_2 adsorption isotherms at 77 K (Figure 1f and Figure S12–S14). The Brunauer–Emmett–Teller (BET) surface area of TTCOF-Zn was calculated to be $564.6\text{ m}^2\text{ g}^{-1}$. Moreover, the total pore volume ($0.93\text{ cm}^3\text{ g}^{-1}$) and the pore sizes (1.02 and 1.56 nm) for TTCOF-Zn are in conformity with the theoretical results. The chemical stability of TTCOF-Zn was examined by immersing it into different solvents at room temperature. The FTIR spectra and PXRD patterns indicated its structural robustness (Figures S15 and S16). The thermal stabilities of TTCOF-M were confirmed by thermogravimetric analysis (Figure S17–S20), which showed no obvious change up to 300°C .

The morphology of TTCOF-M was characterized using scanning electron microscopy (SEM) and transmission electron microscopy (TEM), which shows that TTCOF-Zn is composed of hollow spheres with 1–3 μm in diameter and self-assembled small rectangular sheet-shaped crystals with about 0.1–0.2 μm in length (Figure 2a and Figures S21 and S22). The fast Fourier transformation image of high-resolution transmission electron microscopy (HR-TEM) showed the hexagonal pore structure arrangement along the 001 crystal axis, which can also manifest the AA-stacking mode of the 2D TTCOF-Zn structure (Figure 2b). Additionally, energy-dispersive X-ray spectroscopy (EDS) analysis reveals that C, N, S, and Zn are uniformly distributed over TTCOF-Zn (Figure S23–S25). The Zn content in TTCOF-Zn was determined to be circa 4.3 wt% by inductively coupled plasma (ICP) optical emission spectrometry (Table S1).

The visible light-driven (420–800 nm) photocatalytic CO_2RR was conducted under pure CO_2 (1.0 atm, 298 K) atmosphere in a CO_2 -saturated H_2O solution, without additional photosensitizer (PS) and sacrificial agents (SA). It is well known that the CO_2 absorption ability is an important factor for CO_2RR photocatalysts.^[15] The CO_2 adsorption isotherms of TTCOFs were measured and determined to be 28, 52, 42, and $38\text{ cm}^3\text{ g}^{-1}$ for TTCOF-2H/Zn/Ni/Cu, respectively (Figure 2c). The increased CO_2 adsorption capacity of TTCOF-Zn/Ni/Cu compared to the host TTCOF-2H should be attributed to the strong affinity between the metal ion and CO_2 molecule.^[16] At the same time, water vapor adsorption tests for TTCOFs showed characteristic type II isotherm (Figure S26–S29), which indicated that the internal pore structure and external surface of these materials are accessible to water.^[17] This hydrophilicity fact can also be demonstrated by water contact angles tests showing angles of $22\text{--}45^\circ$ (Figure S30).

Previous studies have revealed that to achieve photocatalytic CO_2RR with H_2O , the photocatalyst is required to have a more negative conduction band minimum (CBM) potential than the CO_2 reduction potential (CO/CO_2 , theoretically -0.53 V vs. NHE, pH 7 and -4.37 eV vs. E_v , vacuum level) as well as more positive valence band maximum (VBM) potential than the H_2O oxidation potential ($\text{O}_2/\text{H}_2\text{O}$, theoretically 0.82 V vs. NHE, pH 7 and -5.67 eV vs. E_v).^[2b] UV/Vis diffuse reflectance spectroscopy (DRS) and with ultraviolet

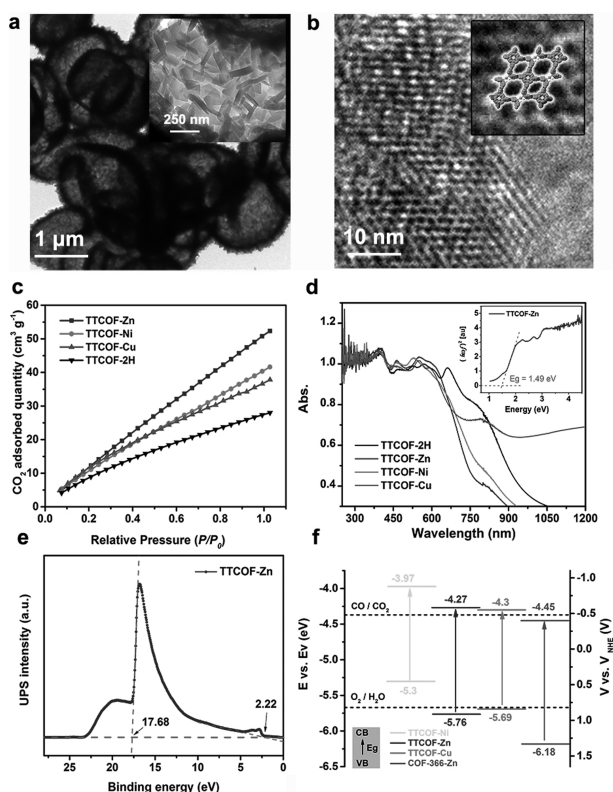


Figure 2. a) TEM images and b) HRTEM image of TTCOF-Zn, the pores are highlighted in the inset. c) CO₂ adsorption curves of TTCOF-M measured at 298 K. d) Solid-state UV/Vis spectra of TTCOF-M. e) UPS spectra of TTCOF-Zn. f) Band structure diagram for TTCOF-M and COF-366-Zn.

photoelectron spectroscopy (UPS) were conducted to determine the electronic properties of TTCOF-M. These TTCOFs exhibited a broad visible-light absorption range, and the corresponding band gaps (E_g) were determined to be 1.15, 1.49, 1.33, and 1.39 eV for TTCOF-2H/Zn/Ni/Cu by Tauc plots (Figure 2d inset and Figures S31–S33), respectively, suggesting the characteristics of a semiconductor.^[18] The VBM of TTCOF-Zn was calculated to be -5.76 eV (vs. E_v) from the UPS pattern (Figure 2e) and the CBM was thus calculated to be -4.27 eV (vs. E_v). Mott–Schottky measurements were also conducted to determine the band positions of TTCOF-M (Figure S36), which were consistent with the results extracted from UPS. It is clear that the CBM of TTCOF-Zn is more negative than the standard reduction potential of CO/CO₂ and its VBM is more positive than the oxidation potential of O₂/H₂O, suggesting its ability to integrate CO₂ reduction with H₂O oxidation reactions. Similarly, the electronic properties of other COFs and COF-366-Zn were also obtained by the above-mentioned methods (Figures S34–S35 and S37–S44) and the energy-band alignment results were presented in Figure 2f. TTCOF-Zn/Cu, owing to the matched band structure, fulfilled the artificial photosynthesis with H₂O oxidation, while TTCOF-Ni and COF-366-Zn were considered to be unsuitable.

The photocatalytic reactions were first carried out with TAPP-M monomers, no observable product was detected.

When TTCOFs were used as photocatalysts, TTCOF-Zn showed the highest CO evolution of $12.33 \mu\text{mol}$ under visible light illumination after 60 h, which was higher than that of TTCOF-Cu ($8.65 \mu\text{mol}$) and TTCOF-Ni ($0.462 \mu\text{mol}$) (Figure 3a, black). Each data point is an average of three separate trials performed under the same conditions, and the standard deviation of these measurements is indicated by the error bar. At the same time, the yield of O₂ was also detected (Figure 3a and Figures S45 and 46). As expected, the CO/O₂ ratio is about 2:1. Only the COFs exhibit prominent photocatalytic activity, and the mechanisms behind this are discussed below. Moreover, the time-dependent CO output increased almost linearly with irradiation time for the TTCOF-Zn catalyst (Figure 3b). To further confirm the photocatalytic activity of TTCOFs, a series of control experiments were performed (Table S2). These results showed that no other gaseous products (except CO and O₂) were detected by GC, and trace liquid products could be detected in the liquid phase by ¹H NMR (Figure S48), suggesting its high CO selectivity. The isotope labeling experiments were performed to ascertain the carbon and oxygen sources of photochemical products. Firstly, we use ¹³CO₂ as substrates, ¹³CO ($m/z = 29$) was finally detected by using mass spectrometry, which confirmed that the produced CO originated from the reactant CO₂ instead of decomposition of catalyst (Figure 3c and Figure S49–50). Moreover, when H₂¹⁸O was used as reaction solution, ¹⁸O₂ ($m/z = 36$) and ¹⁸O¹⁶O ($m/z = 34$) were detected in the gas phase after the reaction (Figure S51), confirming that the generated ¹⁸O₂ stemmed from the oxidation of H₂¹⁸O. Additionally, our catalyst system can maintain at least five cycles (Figure 3d). The crystallinity and structural integrity of TTCOF-Zn were retained after the reaction, as confirmed by PXRD, FTIR, and XPS characterizations (Figure S52–S54). All of this confirmed that TTCOF-Zn materials are

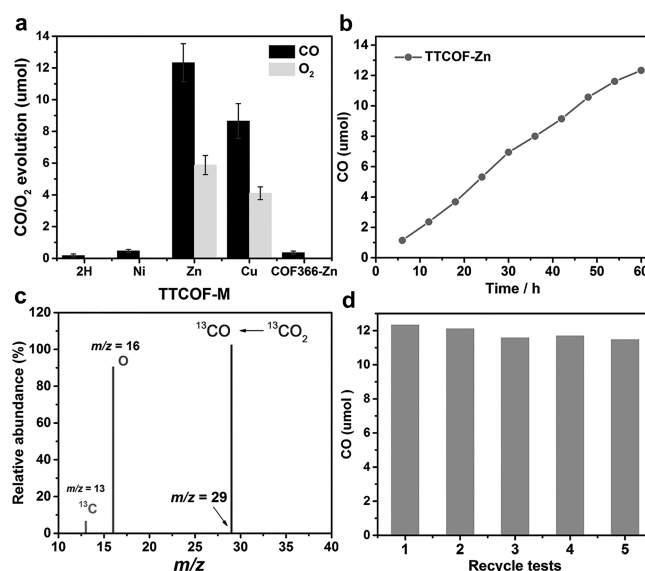


Figure 3. a) CO₂RR performance of TTCOF-M and COF366-Zn. b) Time-dependent CO production performance using TTCOF-Zn as photocatalyst. c) MS of ¹³CO produced from the photocatalytic reduction of ¹³CO₂. d) Durability tests of TTCOF-Zn.

efficient and selective heterogeneous photocatalysts for combining CO₂ photoreduction with H₂O photooxidation.

Many characterization methods were performed to investigate the reasons for the different performances of these photocatalysts. Incident-photon-to-current conversion efficiency (IPCE) analysis was used to examine the photoinduced electron transfer (PET) efficiency. These results showed that the photo-current responses for TTCOF-M (metalloporphyrin) are much stronger than that of TTCOF-2H (metal-free) (Figure S55), indicating a more efficient separation of photogenerated electron-hole pairs by ligand-to-metal charge-transfer effect. Additionally, photoluminescence (PL) and time-resolved fluorescence decay techniques were conducted to investigate the charge separation behaviors. The PL intensity of TTCOF-Zn was significantly quenched (Figure S56) compared to molecular TAPP-Zn and TTF. At the same time, TTCOF-Zn has a longer fluorescence lifetime ($\tau_1 = 53.45 \pm 1.6$ ns) than that of TAPP-Zn (45.57 ± 0.76 ns) (Figures S57 and S58), suggesting that the efficient electron transfer within COF is favorable for the promotion of charge separation efficiency.

Based on the above experiments and analysis, an intrinsic mechanism was proposed to explain the CO₂RR process with H₂O oxidation: driven by visible-light irradiation, the PET process takes place from the TTF moiety (HOMO center) to the TAPP moiety (LUMO center) after absorbing photons, the excited electrons then move to catalytically active sites (Zn/Cu in TAPP) and are used for CO₂ reduction. Meanwhile, the photogenerated holes in TTF are capable of oxidizing H₂O to O₂, by which the catalytic system gains electrons from H₂O to keep the charge balance (Figure 4a).

DFT calculation study were applied to understand the photo-excitation process and catalytic reaction mechanisms. The low-lying electronic transitions in the TTCOF framework are shown in Figure 4b, and the inset demonstrates the first excitation contribution, that is, from HOMO to LUMO. As we expected, the well-known electron-donating TTF fragment dominates the HOMO while the LUMO is mainly contributed by the TAPP part. Therein, the PET process can readily occur by light irradiation, which further forms photo-generated electrons located on the TAPP-M (formed TAPP-M⁻) and photogenerated holes centered at the TTF unit (formed TTF⁺). For the hole-doped TTF⁺, the spin density mostly locates on linker C=C and the S atoms (Figure S59),

indicating that the H₂O oxidation process can be conducted on both sites. For the electrons located TAPP-M⁻, the CO₂ reduction reaction will occur on the metal ion center. This result confirmed the proposed mechanism.

In summary, a series of 2D COFs were synthesized and used as photocatalysts to reduce CO₂ with H₂O as electron donor, without additional PS, SA, and noble metal co-catalyst. Thanks to the effective covalent coupling between porphyrin and tetrathiafulvalene molecules within TTCOFs, the electron-hole pairs induced by visible-light irradiation can be separated and transferred efficiently for CO₂ reduction and H₂O oxidation reactions. TTCOF-Zn shows the highest photocatalytic CO production of 12.33 μ mol with circa 100% selectivity and superior durability under our experimental conditions. This is the first report of rationally designed crystalline COF system applied for the selective photoreduction of CO₂ with H₂O as electron donor. Moreover, we offer a more straightforward and clearer crystalline evidence for understanding the structure-function relationship of heterogeneous photocatalysts. Our research provides a new insight into the design of next generation crystalline photocatalysts for artificial photosynthesis of CO₂ with H₂O.

Acknowledgements

This work was financially supported by NSFC (No. 21622104, 21701085, 21871141 and 2187114); the NSF of Jiangsu Province of China (No.BK20171032); the Natural Science Research of Jiangsu Higher Education Institutions of China (No.17KJB150025); Priority Academic Program Development of Jiangsu Higher Education Institutions and the Foundation of Jiangsu Collaborative Innovation Center of Biomedical Functional Materials.

Conflict of interest

The authors declare no conflict of interest.

Keywords: CO₂ photoreduction · covalent organic frameworks · electron transfer · H₂O photooxidation

How to cite: *Angew. Chem. Int. Ed.* **2019**, *58*, 12392–12397
Angew. Chem. **2019**, *131*, 12522–12527

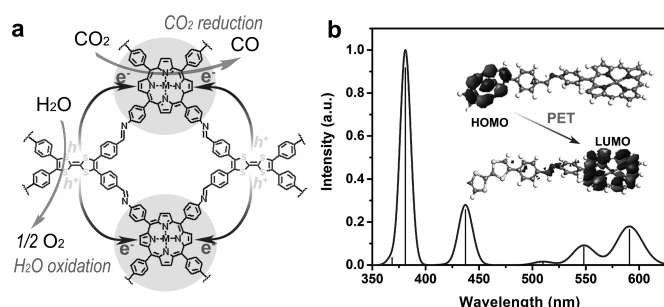


Figure 4. a) Schematic of the mechanism of TTCOF-M CO₂RR with H₂O oxidation. b) Theoretical simulation UV/Vis DRS of TTCOF-Zn and scheme of PET route under light excitation (inset).

- [1] a) J. Barber, P. D. Tran, *J. R. Soc. Interface* **2013**, *10*, 20120984; b) S. J. Davis, K. Caldeira, H. D. Matthews, *Science* **2010**, *329*, 1330–1333.
- [2] a) X. Chang, T. Wang, J. Gong, *Energy Environ. Sci.* **2016**, *9*, 2177–2196; b) X. Liu, S. Inagaki, J. Gong, *Angew. Chem. Int. Ed.* **2016**, *55*, 14924–14950; *Angew. Chem.* **2016**, *128*, 15146–15174.
- [3] a) K. Maeda, *ACS Catal.* **2013**, *3*, 1486–1503; b) H. Li, W. Tu, Y. Zhou, Z. Zou, *Adv. Sci.* **2016**, *3*, 1500389.
- [4] a) S. Das, P. Heasman, T. Ben, S. Qiu, *Chem. Rev.* **2017**, *117*, 1515–1563; b) Y. Zhang, J. Duan, D. Ma, P. Li, S. Li, H. Li, J. Zhou, X. Ma, X. Feng, B. Wang, *Angew. Chem. Int. Ed.* **2017**, *56*, 16313–16317; *Angew. Chem.* **2017**, *129*, 16531–16535.
- [5] N. C. Burtch, H. Jasuja, K. S. Walton, *Chem. Rev.* **2014**, *114*, 10575–10612.

- [6] N. Huang, P. Wang, D. Jiang, *Nat. Rev. Mater.* **2016**, *1*, 16068.
- [7] S. Lin, C. S. Diercks, Y. B. Zhang, N. Kornienko, E. M. Nichols, Y. Zhao, A. R. Paris, D. Kim, P. Yang, O. M. Yaghi, C. J. Chang, *Science* **2015**, *349*, 1208–1213.
- [8] A. Nagai, Z. Guo, X. Feng, S. Jin, X. Chen, X. Ding, D. Jiang, *Nat. Commun.* **2011**, *2*, 536.
- [9] S. Wan, F. Gándara, A. Asano, H. Furukawa, A. Saeki, S. K. Dey, L. Liao, M. W. Ambrogio, Y. Y. Botros, X. Duan, S. Seki, J. F. Stoddart, O. M. Yaghi, *Chem. Mater.* **2011**, *23*, 4094–4097.
- [10] a) S. Yang, W. Hu, X. Zhang, P. He, B. Pattengale, C. Liu, M. Cendejas, I. Hermans, X. Zhang, J. Zhang, J. Huang, *J. Am. Chem. Soc.* **2018**, *140*, 14614–14618; b) Y. Fu, X. Zhu, L. Huang, X. Zhang, F. Zhang, W. Zhu, *Appl. Catal. B* **2018**, *239*, 46–51.
- [11] a) T. Kojima, T. Honda, K. Ohkubo, M. Shiro, T. Kusakawa, T. Fukuda, N. Kobayashi, S. Fukuzumi, *Angew. Chem. Int. Ed.* **2008**, *47*, 6712–6716; *Angew. Chem.* **2008**, *120*, 6814–6818; b) K. Kilså, J. Kajanus, A. N. Macpherson, J. Martensson, B. Albinsson, *J. Am. Chem. Soc.* **2001**, *123*, 3069–3080.
- [12] a) C. M. Davis, Y. Kawashima, K. Ohkubo, J. M. Lim, D. Kim, S. Fukuzumi, J. L. Sessler, *J. Phys. Chem. C* **2014**, *118*, 13503–13513; b) A. Jana, S. Bähring, M. Ishida, S. Goeb, D. Canevet, M. Salle, J. O. Jeppesen, J. L. Sessler, *Chem. Soc. Rev.* **2018**, *47*, 5614–5645; c) C. K. Graetzel, M. Graetzel, *J. Phys. Chem.* **1982**, *86*, 2710–2714.
- [13] P. Shao, J. Li, F. Chen, L. Ma, Q. Li, M. Zhang, J. Zhou, A. Yin, X. Feng, B. Wang, *Angew. Chem. Int. Ed.* **2018**, *57*, 16501–16505; *Angew. Chem.* **2018**, *130*, 16739–16743.
- [14] S. Y. Ding, J. Gao, Q. Wang, Y. Zhang, W. G. Song, C. Y. Su, W. Wang, *J. Am. Chem. Soc.* **2011**, *133*, 19816–19822.
- [15] H. Zhang, J. Wei, J. Dong, G. Liu, L. Shi, P. An, G. Zhao, J. Kong, X. Wang, X. Meng, *Angew. Chem. Int. Ed.* **2016**, *55*, 14310–14314; *Angew. Chem.* **2016**, *128*, 14522–14526.
- [16] a) H.-Q. Xu, J. Hu, D. Wang, Z. Li, Q. Zhang, Y. Luo, S.-H. Yu, H.-L. Jiang, *J. Am. Chem. Soc.* **2015**, *137*, 13440–13443; b) S. Li, Y. Dong, J. Zhou, Y. Liu, J. Wang, X. Gao, Y. Han, P. Qi, B. Wang, *Energy Environ. Sci.* **2018**, *11*, 1318–1325.
- [17] X. Wang, L. Chen, S. Y. Chong, M. A. Little, Y. Wu, W.-H. Zhu, R. Clowes, Y. Yan, M. A. Zwijnenburg, R. S. Sprick, A. I. Cooper, *Nat. Chem.* **2018**, *10*, 1180–1189.
- [18] G. Zhang, Z. A. Lan, L. Lin, S. Lin, X. Wang, *Chem. Sci.* **2016**, *7*, 3062–3066.

Manuscript received: June 3, 2019

Revised manuscript received: June 24, 2019

Accepted manuscript online: July 3, 2019

Version of record online: August 8, 2019